Macromolecules

Article

pubs.acs.org/Macromolecules

Effects of Electric Charge on the Interfacial Tension between Coexisting Aqueous Mixtures of Polyelectrolyte and Neutral Polymer

Mark Vis,*[,†] Vincent F. D. Peters,[†] Edgar M. Blokhuis,[‡] Henk N. W. Lekkerkerker,[†] Ben H. Erné,*[,†] and R. Hans Tromp[†,§]

[†]Van 't Hoff Laboratory for Physical and Colloid Chemistry, Debye Institute for Nanomaterials Science, Utrecht University, Padualaan 8, 3584 CH Utrecht, The Netherlands

[‡]Supramolecular & Biomaterials Chemistry, Leiden Institute of Chemistry, Leiden University, Einsteinweg 55, 2333 CC Leiden, The Netherlands

[§]NIZO food research, Kernhemseweg 2, 6718 ZB Ede, The Netherlands

Supporting Information

ABSTRACT: Upon demixing, an aqueous solution of a polyelectrolyte and an incompatible neutral polymer yields two phases separated by an interface with an ultralow tension. Here, both in theory and experiment, we study this interfacial tension in detail: how it scales with the concentrations of the polymers in the two phases and how it is affected by the interfacial difference in the electrical potential. Experiments are performed on an aqueous model system of uncharged dextran and charged nongelling gelatin. The experimental tension scales to the power ~3 with the tie-line length in the phase diagram of demixing, in agreement with mean-field theory where space is filled with a binary mixture of polymer blobs. The interfacial electrical potential difference is experimentally found to decrease the interfacial tension in a way that is consistent with Poisson−Boltzmann theory inspired from Frenkel and Verwey−Overbeek.

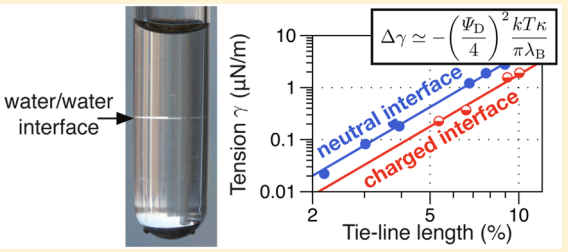

INTRODUCTION

When aqueous solutions of polymers are mixed, phase separation is a commonly observed phenomenon.[1−4] It yields phases that differ in the concentrations of the polymers. The interface between the phases is not abrupt, but there are gradients in the relative composition and the total concentration of the polymers. A particularity of phase separating solutions—as opposed to phase separated blends—results from the osmotic compressibility of the solutions: compared to the bulk phases, the interfacial region is diluted by uptake of solvent.[5] In the case of charged polymers, there is also an interfacial gradient in the electric charge density, corresponding to an interfacial electric potential step. This is the so-called Donnan potential,[6,7] and its effect on the interfacial tension is the subject of this paper.

The main conditions for phase separation are a sufficient concentration and a sufficient degree of polymerization. These two factors often make the unfavorable mixing enthalpy dominate over the small mixing entropy of two types of polymer. Phase separation is also affected by the presence of charge on the polymers.[8] For instance, when one of the polymers is charged and the other is uncharged, phase separation becomes entropically more unfavorable due the accumulation of counterions in one of the phases—necessary for charge neutrality. In order to increase entropy, the positive and negative salt ions spread across the interface to different extents; the buildup of charge separation halts the spreading. The accompanying electric potential difference is the Donnan potential. It has the same origin as the well-known membrane potential found in living cells and dialysis membranes. However, in our case, the charged interface is formed spontaneously and in equilibrium with the bulk phases; moreover, the interfacial electric potential step is relatively small, typically less than 10 mV,[9] as compared to 40−60 mV for the membranes of living cells.

The electric interfacial potential step contributes negatively to the interfacial tension due to the spontaneous formation of interfacial electrical double layers. In certain scenarios, the interfacial tension may become so low that it is favorable for the system to increase spontaneously its interfacial area and to form microdomain structures.[10−12] The question at the outset of the present work was whether the measured interfacial potential step can be quantitatively related to the measured interfacial tension and the phase diagram of demixing, with varying charge density and salt concentration. The experimental system studied here is an aqueous solution of the polysaccharide dextran, which is uncharged, and the protein fish gelatin, which is nongelling and weakly charged, to an extent set by the pH. This is a convenient model system,[13] and it is also representative of many approaches for water structuring used in the food industry.[14] For this system, we previously showed in

Received: July 28, 2015
Published: September 22, 2015

DOI: 10.1021/acs.macromol.5b01675
Macromolecules 2015, 48, 7335−7345

a Letter that the change of the interfacial tension due to charge on one of the polymers is well described by Poisson−Boltzmann theory.[15] Here, we investigate how the magnitude and scaling of the tension of the uncharged interface compare with theory. Additionally, we give a detailed derivation of the theory presented in ref 15 and, moreover, in the Appendix we give an alternative derivation based directly on the free energy of the ions.

The outline of this paper is as follows. In the first part of the Theory section, expressions are given for the interfacial tension on the basis of the interfacial profiles of the relative composition and total concentration of polymers in solution. In the second part, the contribution to the interfacial tension from a charge density profile is calculated from the free energy density of two coupled electric double layers. Subsequently, the experimental procedures with which we obtained interfacial electric potentials, interfacial tensions, and phase compositions are described. Finally, the experimental results and the extent to which they agree with theory are discussed.

THEORY

This section starts with the calculation of the interfacial tension of demixed solutions of neutral polymers on the basis of the blob model. Next, the change in the tension of a liquid/liquid interface is calculated in the case that it carries an electrical potential difference, using Poisson−Boltzmann theory. A list of symbols is given in the Supporting Information.

Interfacial Tension of a Demixed Solution of Two Polymers. Via the blob model, we will describe a solution of two uncharged polymers A and B that are identical except for the repulsive interaction between the two. By treating the solvent implicitly, the three-component system is reduced to an effective two-component system, which makes the blob model convenient for aqueous two-phase systems.[5,16−19] Following refs 5 and 16−19, we will discuss first the free energy resulting from the blob model for a single phase of a given relative composition and total polymer concentration. This will be extended subsequently in order to account for the presence of an interface, by allowing gradients in composition and concentration. The interfacial tension follows by finding gradients across the interface such that the excess grand free energy is minimized.

In the blob model, a polymer consisting of N segments forms N_b solvent-filled blobs of characteristic size ξ. The blobs form an ideal chain. The volume fraction of blobs of polymer A and B are ϕ and $1 - \phi$, respectively, and the total number of monomers (of A and B combined) per unit volume is c. The free energy per unit volume is given by[5,16−19]

$$\frac{F}{VkT} = \frac{1}{\xi^3(c)}\left[\frac{\phi}{N_b(c)}\ln\phi + \frac{1-\phi}{N_b(c)}\ln(1-\phi) + u(c)\phi(1-\phi) + K\right] \quad (1)$$

where $u(c)$ represents the concentration-dependent repulsive interaction between the two polymers and $K = 0.024$[16] represents the free energy of mixing within a blob. The blob size, the number of blobs per polymer chain, and the interaction potential are given by, respectively, $\xi(c) \simeq 0.43R_g(c/c^*)^{-\nu/(3\nu-1)}$, $N_b(c) = N/[c\xi^3(c)]$, and $u(c) \simeq u_{crit}(c/c_{crit})^{\chi/(3\nu-1)}$.

The scaling exponents are $\nu = 3/5$ and $\chi = 0.22$ for a good solvent. The overlap concentration is defined as $c^* \equiv N/\left(\frac{4}{3}\pi R_g^3\right)$, with R_g being the radius of gyration of the polymers. c_{crit} is defined as the lowest concentration where phase separation is observed experimentally, and u_{crit} is the interaction at this concentration. u_{crit} is the only fit parameter of the model.

In the case that eq 1 has two inflection points as a function of ϕ, the system can reduce its free energy by demixing into two phases, α and β, one rich in polymer A and one in B. The concentration at which the composition of the two phases becomes identical, the critical point, can be varied by changing the interaction parameter u_{crit} in order to match the critical point in the experiments. For comparison of calculations with experiments, the monomer concentration c is converted to the mass fraction w. We assume the densities and molar masses listed in Table 1 as well as additivity of volume. On the basis of the mass fractions, the tie-line length L can be calculated. The tie-line length is a measure of the composition difference between the two phases, and it is given by $L \equiv [(w_\alpha^A - w_\beta^A)^2 + (w_\alpha^B - w_\beta^B)^2]^{1/2}$, where the superscripts refer to the different polymers and the subscripts to the different phases. The tie-line length serves as the order parameter to compare theory and experiments. A list of parameters used in the present calculations is given in Table 1.

Table 1. Values of the Parameters Used in the Calculations

parameter	value	description
ν	3/5	scaling parameter[16]
χ	0.22	scaling parameter[16]
K	0.024	constant related to free energy of mixing within a blob[16]
R_g	9.3 nm	radius of gyration, taken to be R_g of dextran[20]
$M_{w,polymer}$	100 kg/mol	average molar mass of dextran and gelatin
$M_{w,monomer}$	0.1 kg/mol	approximate molar mass of a monomer
N	1000	degree of polymerization, given by $M_{w,polymer}/M_{w,monomer}$
$\rho_{polymer}$	1496 kg/m^3	average aqueous densities of dextran and gelatin
$\rho_{solvent}$	998 kg/m^3	density of water at 20 °C[21]
w_{crit}	0.063	experimental critical mass fraction of phase separation
c_{crit}	3.9×10^{26} m^{-3}	calculated from w_{crit}
u_{crit}	0.03	interaction at c_{crit}; fit parameter

The interfacial tension can be calculated by allowing for ϕ and c to depend on position and adding the appropriate gradient terms to eq 1. Following Broseta and co-workers[5,16,17] (see also refs 18 and 19), the free energy per unit area with a planar interface between phases α and β is given by

$$\frac{F}{AkT} = \int_{-\infty}^{\infty} dz\left[\frac{\phi}{N_b\xi^3}\ln(\phi) + \frac{1-\phi}{N_b\xi^3}\ln(1-\phi) + \frac{u}{\xi^3}\phi(1-\phi) + \frac{K}{\xi^3} + \frac{\phi'^2}{24\xi\phi} + \frac{\phi'^2}{24\xi(1-\phi)} + \frac{c'^2}{24\xi c^2}\right] \quad (2)$$

Both ϕ and c are now functions of the distance z to the interface, and the primed symbols denote derivatives with

DOI: 10.1021/acs.macromol.5b01675
Macromolecules 2015, 48, 7335−7345

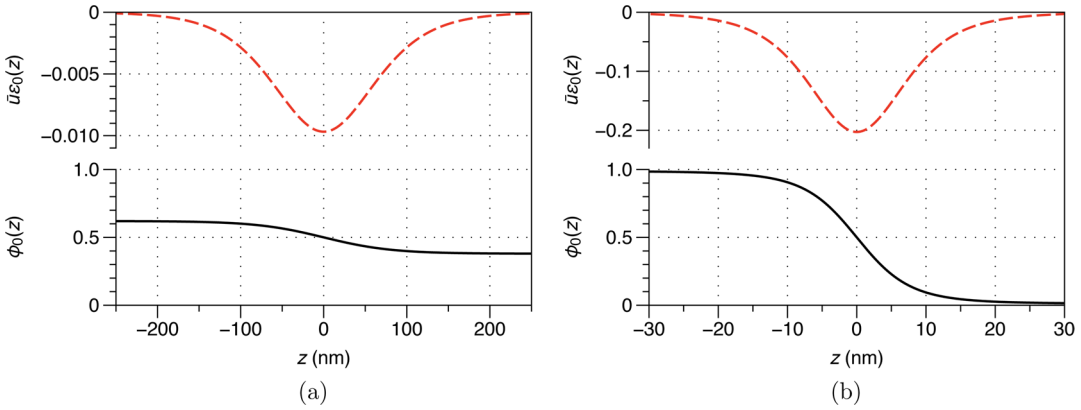

Figure 1. Equilibrium profiles of the concentration change $\bar{u}\epsilon_0(z)$ and the polymer composition $\phi_0(z) = [1+\eta_0(z)]/2$ for (a) w = 6%, where γ = 0.06 μN/m, and (b) w = 10%, where γ = 25 μN/m. The interfacial region goes through a minimum in the total polymer concentration and extends over increasingly large distances as one nears the critical point of demixing. The blob sizes are 3.4 (a) and 2.3 nm (b). The calculations were made on the basis of eqs 1−8 and Table 1.

respect to z. Note that since N_b, ξ, and u are functions of c, they are now also functions of z.

For convenience we define $\phi(z) \equiv [1 + \eta(z)]/2$ and $c(z) \equiv \bar{c}[1 + \bar{u}\epsilon(z)]$, where $\bar{c}$ and $\bar{u}$ represent the values of c and u in the bulk where gradients are absent. The deviation of $\phi(z)$ from 1/2 is expressed by $\eta(z)$, and the relative deviation of $c(z)$ from $\bar{c}$ is given by $\bar{u}\epsilon(z)$. Let us assume that $\bar{u}\epsilon(z)$ is small everywhere, so that we can approximate the concentration-dependent quantities to second order in $\bar{u}\epsilon(z)$, and that the gradients in composition are independent of the gradients in concentration. Further, $\omega \equiv \bar{N}_b\bar{u}$ and $x \equiv z/D_\infty$ (with $D_\infty \equiv \bar{\xi}/\sqrt{6\bar{u}}$) are defined, where similarly $\bar{N}_b$ and $\bar{\xi}$ represent bulk values. The excess grand free energy of the interface, per unit area, is then found by subtracting the free energies of each bulk phase given by eq 1 from eq 2:

$$\frac{\Omega}{AkT} = \frac{\sqrt{6\bar{u}}}{\bar{\xi}^2}\int_{-\infty}^{\infty} dx\left\{\frac{1+\eta}{2\omega}\ln(1+\eta) + \frac{1-\eta}{2\omega}\ln(1-\eta) - \frac{\eta^2}{4} + \frac{\eta'^2}{4(1-\eta^2)} + \frac{1+\eta}{2\omega}\ln[\bar{u}\epsilon(1+\eta)] + \frac{1-\eta}{2\omega}\ln[\bar{u}\epsilon(1-\eta)] - \frac{3\nu+\chi}{4(3\nu-1)}\eta^2\bar{u}\epsilon + \frac{3\nu K}{2(3\nu-1)^2}\bar{u}\epsilon^2 + \frac{\bar{u}^2}{4}\epsilon'^2 - \mu_\eta\eta - \mu_\epsilon\bar{u}\epsilon + \bar{p}\right\} \quad (3)$$

where the bulk pressure and exchange chemical potential are given by

$$\bar{p} = -\frac{\bar{\eta}^2}{4} - \frac{1}{2\omega}\ln(1-\bar{\eta}^2) \quad (4)$$

$$\mu_\epsilon = \frac{1+\bar{\eta}}{2\omega}\ln(1+\bar{\eta}) + \frac{1-\bar{\eta}}{2\omega}\ln(1-\bar{\eta}) - \frac{3\nu+\chi}{4(3\nu-1)}\bar{\eta}^2 \quad (5)$$

and $\mu_\eta = 0$ because the phase separation is symmetric. The bulk composition $\bar{\eta}$ of the coexisting phases is found from the condition:

$$\frac{1}{\omega}\ln\left(\frac{1+\bar{\eta}}{1-\bar{\eta}}\right) - \bar{\eta} = 0 \quad (6)$$

where the compositions of phases α and β are given by $\eta_\alpha = \bar{\eta}$ and $\eta_\beta = -\bar{\eta}$.

The optimal composition profile $\eta(x)$ that minimizes the interfacial tension is denoted as $\eta_0(x)$. We assume no effect of the concentration profile on the composition profile, so $\epsilon(x)$ can be set to zero. The composition profile is found by numerically solving the following differential equation, obtained by using the Euler−Lagrange equation:

$$\frac{\eta_0'(x)^2}{4[1-\eta_0(x)^2]} = \frac{1+\eta_0(x)}{2\omega}\ln[1+\eta_0(x)] + \frac{1-\eta_0(x)}{2\omega}\ln[1-\eta_0(x)] - \frac{\eta_0(x)^2}{4} + \bar{p} \quad (7)$$

for which the boundary condition that $\eta_0(x) = 0$ at $x = 0$ is used. Once a solution for $\eta_0(x)$ is known, this can be used to find the optimal profile of $\epsilon(x)$, $\epsilon_0(x)$, by solving

$$\frac{\bar{u}}{2}\epsilon_0''(x) = \frac{1+\eta_0(x)}{2\omega}\ln[1+\eta_0(x)] + \frac{1-\eta_0(x)}{2\omega}\ln[1-\eta_0(x)] + \frac{3\nu K}{(3\nu-1)^2}\epsilon_0(x) - \frac{3\nu+\chi}{4(3\nu-1)}\eta_0(x)^2 - \mu_\epsilon \quad (8)$$

This can be done efficiently numerically using the finite element method, with the boundary conditions that $\epsilon_0'(0) = 0$ and that $\epsilon_0(x)$ goes to zero for large x. Examples of profiles close to and far away from the critical point are given in Figure 1.

The interfacial tension γ is then given by

$$\gamma = \frac{kT}{\bar{\xi}^2}\sqrt{\frac{\bar{u}}{6}} \times (1 - \Delta_1 - \bar{u}\Delta_2) \quad (9)$$

where

DOI: 10.1021/acs.macromol.5b01675
Macromolecules 2015, 48, 7335−7345

$$\Delta_1 = 1 - 2\int_0^{\bar{\eta}} d\eta\ (1-\eta^2)^{-1/2} \times \left[\frac{1+\eta}{2\omega}\ln(1+\eta) + \frac{1-\eta}{2\omega}\ln(1-\eta) - \frac{\eta^2}{4} + \bar{p}\right]^{1/2} \quad (10)$$

$$\Delta_2 = \int_{-\infty}^{\infty} dx\ \epsilon_0(x) \times \left[\frac{-\eta_0'(x)^2}{8(1-\eta_0(x)^2)} + \frac{1+\chi}{8(3\nu-1)}(\eta_0(x)^2 - \bar{\eta}^2)\right] \quad (11)$$

Here, Δ_1 represents the interfacial tension due to an optimal profile in the composition (i.e., the blob volume fraction $\phi(z)$) across the interface, at constant total monomer concentration c. Conform van der Waals theory,[22] this contribution may be calculated without prior knowledge of $\eta_0(x)$; instead, it follows directly from the integral above.

On the other hand, Δ_2 represents a reduction in γ by allowing the total monomer concentration c to vary across the interface, which requires knowledge of both $\eta_0(x)$ and $\epsilon_0(x)$. For parameters matching our experimental system, far away from the critical point, the total monomer concentration at the interface is roughly 20% lower than in bulk and the interfacial zone has a typical width of 10 nm, as is evident from Figure 1b.

The effect of the reduction of the polymer concentration at the interface on the interfacial tension can be found by calculating the ratio

$$\Gamma \equiv \frac{1-\Delta_1-\bar{u}\Delta_2}{1-\Delta_1} \quad (12)$$

This ratio is shown in Figure 2 as a function of the tie-line length L. Far from the critical point, γ is reduced by 15%, but close to the critical point significantly more. Experimentally, L is in the range of 2 to 15%, so the effect of solvent redistribution cannot be neglected and is certainly not constant when varying the tie-line length in this range.

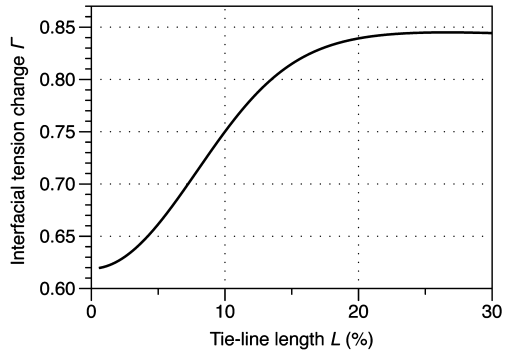

Figure 2. Relative change Γ of the interfacial tension due to solvent redistribution as a function of the tie-line length L, see eq 12.

Interfacial Electrical Potential Difference. In order to capture the effects of an interfacial electrical potential difference on the interfacial tension, the free energy of the electric double layers at the liquid/liquid interface will be calculated using Poisson–Boltzmann theory. This free energy represents a contribution to the interfacial tension and, as these double layers form spontaneously, it is negative. The following derivation closely resembles that found in the books by Verwey and Overbeek[23] and Frenkel[24] for a solid/liquid interface, somewhat adapted in order to account for the presence of two aqueous phases; similar theory has been applied to charged oil/water and water/air interfaces.[25−27]

In general, the Poisson–Boltzmann equation reads as follows

$$\frac{d^2}{dz^2}\left(\frac{e\psi}{kT}\right) = \kappa^2 \sinh\left(\frac{e\psi}{kT}\right) \quad (13)$$

where $\psi = \psi(z)$ is the potential at a distance z from the interface, e is the elementary charge, k is the Boltzmann constant, and T is the absolute temperature. The Debye screening constant is defined as $\kappa = \sqrt{8\pi\lambda_B c_s}$, with c_s the concentration of salt far from the charged interface and $\lambda_B \equiv e^2/(4\pi\epsilon\epsilon_0 kT)$ the Bjerrum length. ϵ is the relative permittivity and ϵ_0 the permittivity of free space.

In terms of the dimensionless potential $\Psi \equiv e\psi/kT$ and dimensionless distance $Z \equiv \kappa z$, the Poisson–Boltzmann equation is written as

$$\frac{d^2\Psi}{dZ^2} = \sinh\Psi \quad (14)$$

With the help of the Poisson–Boltzmann equation, the interfacial charge density can be calculated, which subsequently can be used to calculate the free energy of electrical double layers.

Charge Density of the Electric Double Layer. The water/water interface can be modeled in a way similar to a charged solid surface immersed in a liquid, except that it is regarded as *two* coupled electrical double layers, one in each phase. At this interface, the concentration $c^p(Z)$ of polyelectrolyte gradually changes from c_α^p to c_β^p. We assume that phase α is rich in polyelectrolyte and that the polyelectrolyte itself carries a positive number of charges z (not to be confused with the spatial coordinate z).

Close to the interface, the concentration of polyelectrolyte is either lower (in phase α) or higher (in phase β) than in the bulk. Let us assign to this a local polyelectrolyte excess charge density, $ze(c^p(Z) - c^p_{bulk})$, which can be integrated over Z in order to obtain a surface charge density on either side of the interface. These surface charge densities lead to the formation of a diffuse layer of oppositely charged ions on each side of the interface, thus creating two double layers.

Suppose that far from the interface, the phases have electric potentials given by Ψ_α and Ψ_β. The local concentrations of positive and negative ions are then given by the following Boltzmann distributions:

$$c^+(Z) = c_\alpha \exp[-(\Psi - \Psi_\alpha)] = c_\beta \exp[-(\Psi - \Psi_\beta)] \quad (15)$$

$$c^-(Z) = c_\alpha \exp[\Psi - \Psi_\alpha] = c_\beta \exp[\Psi - \Psi_\beta] \quad (16)$$

with c_α and c_β the salt concentrations in the bulk of phases α and β. The total charge density $\rho_e(Z) \equiv ec^+(Z) - ec^-(Z)$ then becomes

$$\rho_e(Z) = \begin{cases} -2ec_\alpha \sinh(\Psi - \Psi_\alpha) & (Z < 0) \\ -2ec_\beta \sinh(\Psi - \Psi_\beta) & (Z > 0) \end{cases} \quad (17)$$

Here, the assumption is made that we can neglect the polyelectrolyte contribution $zec^p(Z)$ to the total charge density. This turns out to be a valid assumption for our experiments but in the Appendix we discuss the more general situation.

DOI: 10.1021/acs.macromol.5b01675
Macromolecules 2015, 48, 7335−7345

Using the Poisson equation, $2ec_{bulk}\, d^2\Psi/dZ^2 = -\rho_e(Z)$, the Poisson–Boltzmann equation for $\Psi(Z)$ then takes the following form:

$$\frac{d^2\Psi}{dZ^2} = \begin{cases} \sinh(\Psi - \Psi_\alpha) & (Z < 0) \\ \sinh(\Psi - \Psi_\beta) & (Z > 0) \end{cases} \tag{18}$$

A typical electrical potential profile obtained from solving the Poisson–Boltzmann equation is shown in Figure 3.

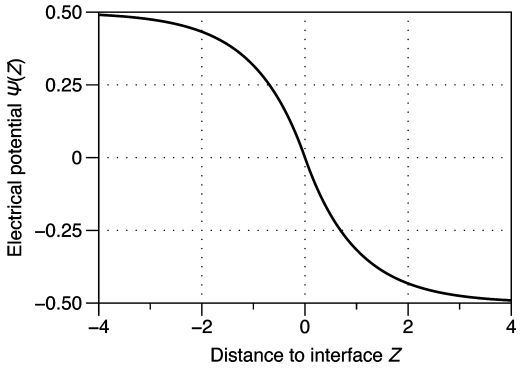

Figure 3. Profile of the dimensionless electrical potential $\Psi \equiv e\psi/kT$ as a function of the dimensionless distance Z to the interface. The profile is obtained by solving eq 18 with $\Psi_\alpha = -\Psi_\beta = 1/2$ and $\Psi(0) = 0$.

The charge per unit area of the diffuse layer σ is found by integrating the charge density $\rho_e(Z)$ in the direction perpendicular to the interface. We find for the net charge in phase α

$$\sigma_\alpha = \int_{-\infty}^{0} dz\, \rho_e(z) = \kappa_\alpha^{-1} \int_{-\infty}^{0} dZ\, \rho_e(Z) = -\frac{e\kappa_\alpha}{2\pi\lambda_{B,\alpha}} \sinh\left(\frac{\Psi_0 - \Psi_\alpha}{2}\right) \tag{19}$$

and for the net charge in phase β

$$\sigma_\beta = \int_{0}^{\infty} dz\, \rho_e(z) = \kappa_\beta^{-1} \int_{0}^{\infty} dZ\, \rho_e(Z) = -\frac{e\kappa_\beta}{2\pi\lambda_{B,\beta}} \sinh\left(\frac{\Psi_0 - \Psi_\beta}{2}\right) \tag{20}$$

where $\Psi_0 = \Psi(0)$ is the potential at the interface. Without loss of generality, we can take $\Psi_0 = 0$. Note that we have allowed for the possibility that the dielectric constants and Debye lengths in the two phases are unequal.

In order to maintain electroneutrality over the two double layers, we have to fulfill the requirement that $\sigma_\alpha + \sigma_\beta = 0$. One may show that this leads to

$$\Psi_\alpha = \ln\left(\frac{\omega + \exp(\Psi_D/2)}{\omega + \exp(-\Psi_D/2)}\right) \tag{21a}$$

$$\Psi_\beta = \ln\left(\frac{\omega \exp(-\Psi_D/2) + 1}{\omega \exp(\Psi_D/2) + 1}\right) \tag{21b}$$

where $\omega \equiv \sqrt{c_\alpha\epsilon_\alpha/(c_\beta\epsilon_\beta)}$ and $\Psi_D \equiv \Psi_\alpha - \Psi_\beta$. For low Ψ_D, eq 21 can be approximated as $\Psi_\alpha \simeq \Psi_D \frac{1}{1+\omega}$ and $\Psi_\beta \simeq -\Psi_D \frac{\omega}{1+\omega}$.

Free Energy of the Electric Double Layer. From the interfacial charge density, the free energy per unit area $f \equiv F/A$ of the double layer in each phase can be calculated. Following the arguments by Verwey and Overbeek[23] and Frenkel,[24] f is in general found from

$$f = \frac{kT}{e} \int_0^\Psi d\Psi'\, \sigma(\Psi') \tag{22}$$

where the prime symbol now denotes a dummy variable. Performing the integration in phase α yields

$$f_\alpha = -\frac{kT\kappa_\alpha}{\pi\lambda_{B,\alpha}}\left[\cosh\left(\frac{\Psi_\alpha}{2}\right) - 1\right] = -\frac{kT\kappa}{\pi\lambda_B}\sqrt{\omega}\left[\cosh\left(\frac{\Psi_\alpha}{2}\right) - 1\right] \tag{23}$$

where *global* values of the Bjerrum and Debye lengths are defined as

$$\lambda_B\kappa^{-1} \equiv \sqrt{\omega}\,\lambda_{B,\alpha}\kappa_\alpha^{-1} \equiv \frac{1}{\sqrt{\omega}}\lambda_{B,\beta}\kappa_\beta^{-1} \tag{24}$$

For low Ψ_α, this is approximated as

$$f_\alpha \simeq -\left(\frac{\Psi_D}{2}\right)^2\left(\frac{1}{1+\omega}\right)^2 \sqrt{\omega}\,\frac{kT\kappa}{2\pi\lambda_B} \tag{25}$$

which introduces an error of less than 2% as long as the value of argument of the hyperbolic cosine is less than 1/2.

A similar derivation can be performed for the double layer in phase β, which results in a free energy per unit area given by

$$f_\beta = -\frac{kT\kappa}{\pi\lambda_B}\frac{1}{\sqrt{\omega}}\left[\cosh\left(\frac{\Psi_\beta}{2}\right) - 1\right] \simeq -\left(\frac{\Psi_D}{2}\right)^2\left(\frac{\omega}{1+\omega}\right)^2 \frac{1}{\sqrt{\omega}}\,\frac{kT\kappa}{2\pi\lambda_B} \tag{26}$$

The sum of f_α and f_β represents the change $\Delta\gamma$ in the interfacial tension due to charge:

$$\Delta\gamma \equiv f_\alpha + f_\beta \simeq -\left(\frac{\Psi_D}{2}\right)^2 \frac{\sqrt{\omega}}{1+\omega}\,\frac{kT\kappa}{2\pi\lambda_B} \tag{27}$$

We now turn our attention to the parameter ω, and more precisely to the factor $\sqrt{\omega}/(1+\omega)$, in eq 27. For a phase-separated aqueous polymer mixture, the dielectric constant of the two phases is approximately the same. However, due to the electric potential difference between the phases, the ionic strengths of the two phases will certainly not be the same, as determined by the Donnan equilibrium $\Psi_D = \ln(c_\beta^+/c_\alpha^+) = \ln(c_\alpha^-/c_\beta^-)$ (see eq A.5 in the Appendix). If we suppose that the (positively charged) polyelectrolyte also contributes to the Debye length, then the concentration of anions in each phase is a good measure for the ionic strength of the phases. We find that ω is then given by $\omega = (c_\alpha^-/c_\beta^-)^{1/2} = \exp(\Psi_D/2)$.

Regardless of the precise value of ω, as long as ω is in the neighborhood of 1, the factor $\sqrt{\omega}/(1+\omega) \simeq 1/2$. Even for $\Psi_D = 1$, where $\omega \simeq 1.65$, the factor $\sqrt{\omega}/(1+\omega)$ deviates only 3% from 1/2. Thus, it seems reasonable to approximate eq 27 as

DOI: 10.1021/acs.macromol.5b01675
Macromolecules 2015, 48, 7335–7345

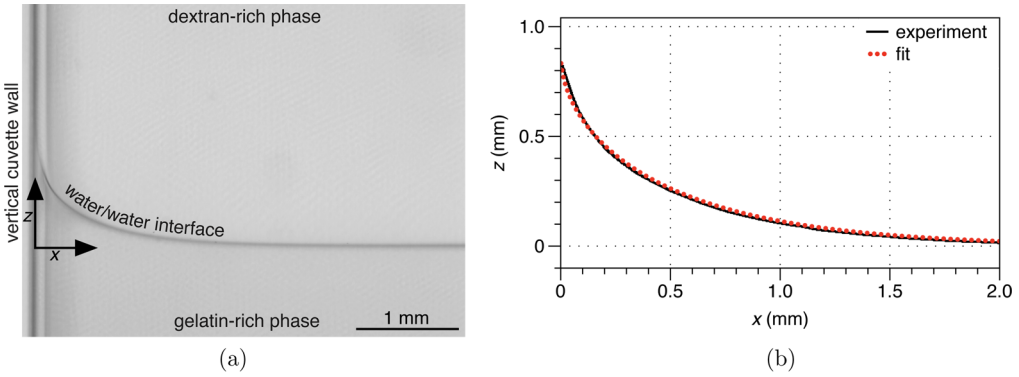

Figure 4. Determination of the interfacial tension.[15] The profile of a water/water interface in a demixed solution of dextran and gelatin (total mass fraction 10%, pH 9.2) is imaged near the wall of a polystyrene cuvette. (a) Micrograph and (b) profile obtained using image analysis together with a fit to eq 29. The density difference is $\Delta\rho = 1.257 \times 10^{-3}$ g/cm^3, and the values resulting from this fit are $l_c = 0.619$ mm and $\gamma = 4.72$ μN/m. The tie-line length in the phase diagram of demixing is 9.87 ± 0.07%.

$$\Delta\gamma \simeq -\frac{kT\kappa}{16\pi\lambda_B}(\Psi_D)^2 \tag{28}$$

Despite the approximations involved, eq 28 describes the change in the interfacial tension very accurately up to $\Psi_D = 1$ ($\psi_D \simeq 25$ mV), where it deviates only a few percent from the exact expression.

From a comparison of this result to that of a solid/liquid interface,[23,24] it is apparent that the resulting formulas are similar. The reduction in the interfacial tension predicted for the liquid/liquid interface is smaller, because the potential difference occurs over a wider region. As the liquid/liquid interface is viewed as two joined double layers, each double layer carries approximately half of the potential drop. The free energy of each double layer scales quadratically with the low potentials involved, so that their free energy is one-fourth that of a single double layer carrying the full potential drop in a solid/liquid interface. However, given that the description of the liquid/liquid interface requires two joined double layers, the decrease in the interfacial tension has half the magnitude compared to the solid/liquid interface.

EXPERIMENTAL SECTION

In this section, the experimental techniques are described: the sample preparation and measurements of the interfacial tensions, the interfacial electrical potential difference, and the composition of the coexisting phases. Detailed accounts on sample preparation, Donnan potential measurements, and the analysis of the composition of the coexisting phases, are given in ref 9.

Sample Preparation. Stock solutions of the uncharged polymer dextran (Sigma-Aldrich, from *Leuconostoc spp.*, average molar mass 100 kDa) were prepared by the dissolving the polymer in Milli-Q water (water filtered with a Millipore apparatus) under gentle mixing. Stock solutions were also prepared of the charged polymer gelatin (Norland Products, kindly provided by FIB Foods, Harderwijk, The Netherlands; fish gelatin type A; gelling temperature 8−10 °C; high molar mass grade, approximately 100 kDa); the gelatin was dissolved in Milli-Q water by magnetic stirring in a warm water bath of 60 °C for 15−30 min. The polydispersity M_w/M_n is about 2.5 for both polymers, where M_w and M_n are the weight- and number-averaged molar masses, respectively. Samples were prepared by mixing the stock solutions and adding Milli-Q water if necessary, resulting in solutions with a 1:1 ratio (by mass) of dextran and gelatin. Samples were centrifuged overnight at 100−200g to achieve two clear macroscopic phases. The charge of gelatin was adjusted by changing the pH, adding dilute hydrochloric acid or sodium hydroxide solutions to the gelatin stock solution. The stock solutions had typical polymer mass fractions of 10−20%. The salt concentration in the resulting samples was approximately 9, 5, and 7 mM at pH 4.8, 6.2, and 9.2, respectively, as deduced from conductivity measurements. In order to study the behavior at increased ionic strength, 50 mM KCl was added. The absolute charge on the gelatin was derived from titration.[28]

Interfacial Tension Measurement. Interfacial tensions were obtained from the capillary length, which was in turn found from an analysis of the static profile of the interface near a vertical wall. This method has been applied before to demixed colloid−polymer mixtures with a similar ultralow interfacial tension.[29] We chose to use this method, as it has been observed that the shear in dynamic methods such as spinning drop could affect the equilibrium phase behavior.[30,31]

First, part of the top phase was collected using a syringe with hypodermic needle. Then the interface was carefully punctured with a fresh needle and syringe, and part of the bottom phase was collected. Part of the isolated bottom phase was placed into a 1 × 1 cm^2 polystyrene cuvette, followed by part of the top phase. The cuvettes were centrifuged at 100−200g for 1 to 2 h in order to remove possible droplets that might have formed during manipulation. A cuvette was mounted in a Nikon Eclipse LV100 Pol that was placed sideways to have a horizontal optical path. Objectives with two or ten times magnification were used, depending on the capillary length, and the images were captured using a QImaging MicroPublisher 5.0 RTV camera. Special attention was paid to ensure that cuvette, microscope, and camera were all level. An example of an image obtained in this way is shown in Figure 4a.

In order to extract the interfacial profiles, the resulting images were analyzed using edge and gradient detection algorithms provided with Mathematica. The profiles were fitted to the following equation, found, e.g., in the book of Batchelor,[32] yielding the capillary length

$$\frac{x(z)}{l_c} = \operatorname{arccosh}\left(\frac{2l_c}{z}\right) - \operatorname{arccosh}\left(\frac{2l_c}{h}\right) - \sqrt{4 - \frac{z^2}{l_c^2}} + \sqrt{4 - \frac{h^2}{l_c^2}} \tag{29}$$

where x is the horizontal distance to the vertical wall, z is the elevation of the interface above the level at large x, h is the contact height (i.e., the elevation of the interface at $x = 0$), and l_c is the capillary length. The capillary length is defined as

$$l_c \equiv \sqrt{\gamma/(\Delta\rho g)} \tag{30}$$

where $\Delta\rho$ is the density difference between the two phases and g is the gravitational acceleration. The contact height h is related to the contact angle θ by $h^2 = 2l_c^2(1 - \sin\theta)$.

For a detailed derivation of eq 29 and more information on the fitting procedure, the reader is referred to the Supporting Information. A comparison of an extracted profile and the resulting fit is given in Figure 4b, which shows excellent agreement.

DOI: 10.1021/acs.macromol.5b01675
Macromolecules 2015, 48, 7335−7345

Extracting the interfacial tension from the capillary length requires knowledge of the density difference between the two phases. The density of the isolated phases was measured using an Anton Paar DMA 5000 oscillating U-tube density meter, which is accurate to 10^{-6} g/cm^3. Such extreme accuracy is necessary, as the density difference between the coexisting phases is typically 10^{-3} g/cm^3 or lower.

The composition of the isolated phases was determined as described below, enabling the measurement of the interfacial tension as a function of the tie-line length. The analysis was performed for the profiles at both the left and right walls of the cuvette. For each side, multiple images were analyzed. The results were averaged per sample and the standard deviations computed.

Donnan Potential Measurement. The electrical potential difference between the two phases—the Donnan potential—was measured electrochemically via the use of reference electrodes[33,34] as described before for the present system.[9] The compositions of the coexisting phases were measured, so that the Donnan potentials could be quantified as a function of the tie-line length.

Analysis of Phase Composition. The compositions of the isolated phases were analyzed using polarimetry. The phases were diluted by a known amount of Milli-Q water in order to contain 1−2% polymer, and the optical rotations were measured in an Anton Paar MCP 500 polarimeter. From the optical rotation at various wavelengths and the dilution factors, the mass fractions of dextran and gelatin in the original sample were obtained for each phase.[9] The measurement principle is based on the fact that both polymers are optically active and that their optical rotary dispersion—the dependence of optical rotation on wavelength—is different. As mentioned in the Theory section, for a given sample, the tie-line length is defined as $L \equiv \sqrt{(w_\alpha^{\mathrm{p}} - w_\beta^{\mathrm{p}})^2 + (w_\alpha^{\mathrm{u}} - w_\beta^{\mathrm{u}})^2}$, where w represents the mass fraction, the superscript "p" refers to the polyelectrolyte gelatin and "u" to the uncharged polymer dextran, and the subscripts α and β refer to the gelatin-rich and dextran-rich phases, respectively. This is shown schematically in the phase diagram depicted in Figure 5.

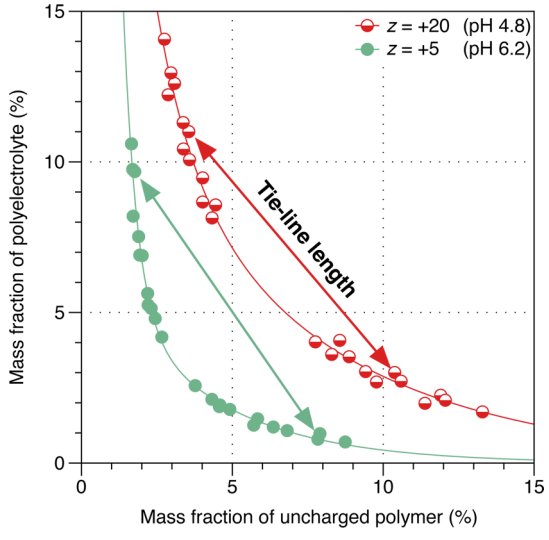

Figure 5. Phase diagrams for the demixing of aqueous solutions of dextran (uncharged polymer) and fish gelatin (polyelectrolyte), measured at polyelectrolyte charges z = +20 (9 mM salt) and z = +5 (5 mM salt).[15] The points are the experimentally measured compositions of the coexisting phases and the solid lines are a guide to the eye. The binodal is shifted away from the origin upon an increase of z. Two tie-lines of approximately equal length are indicated for the two binodals.

RESULTS

In this section, first the phase diagrams will be briefly described, followed by the measurements of the interfacial electrical potential difference. Then, the measured interfacial tensions will be presented. Finally, the measured Donnan potentials and interfacial tensions will be combined in order to calculate the tension of an uncharged interface.

From analyzing the composition of the coexisting phases for many samples, the phase diagrams given in Figure 5 can be obtained. Via the pH, the phase behavior depends strongly on the number of charges z on the polyelectrolyte gelatin: the binodal is shifted away from the origin upon increasing z from +5 to +20. This means that, at the different values of z, phase separation takes place at polymer concentrations that are roughly a factor of 2 different. In order to be able to compare the Donnan potentials and interfacial tensions at these different charges, we will report these as a function of the tie-line length. By analyzing samples of various charges at equal tie-line length, an equal degree of phase separation is implied, making for an apt comparison.

The measured Donnan potentials are shown in Figure 6. A linear correlation of the electrical potential difference is

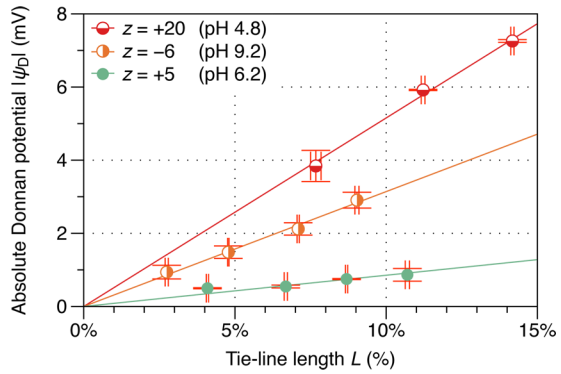

Figure 6. Absolute Donnan potential $|\psi_{\mathrm{D}}|$ published previously[9,15,28] as a function of the tie-line length L. The solid lines represent a linear fit through the origin, used to calculate the effect of charge on the interfacial tension, $\Delta\gamma$, as a function of L using eq 28.

observed with the tie-line length. This is as expected, since the Donnan potential scales linearly with the difference in polyelectrolyte concentration, according to[9,28]

$$\psi_{\mathrm{D}} \simeq \frac{kT}{e}\frac{z\Delta c^{\mathrm{p}}}{2c_{\mathrm{s}}} \tag{31}$$

and the tie-line length is a direct measure of the compositional difference between the two phases. For increased magnitudes of the polyelectrolyte charge z, the magnitude of the Donnan potential is also increased (at a fixed tie-line length), resulting in an increased slope of the plot of $|\psi_{\mathrm{D}}|$ against the tie-line length. For z = −6, the measured Donnan potentials are actually negative, but here we report the absolute value.

Figure 7 shows the measured interfacial tension as a function of the tie-line length. The tensions vary over 4 orders of magnitude and show power-law scaling with the tie-line length, with an exponent of approximately 3.3 independent of the charge z and salt concentration. While the scaling exponent appears to be independent of z, the magnitude of the interfacial tension does depend on z at low ionic strength. Going from z = +5 to z = −6 we observe, if anything, a minute decrease of the

DOI: 10.1021/acs.macromol.5b01675
Macromolecules 2015, 48, 7335−7345

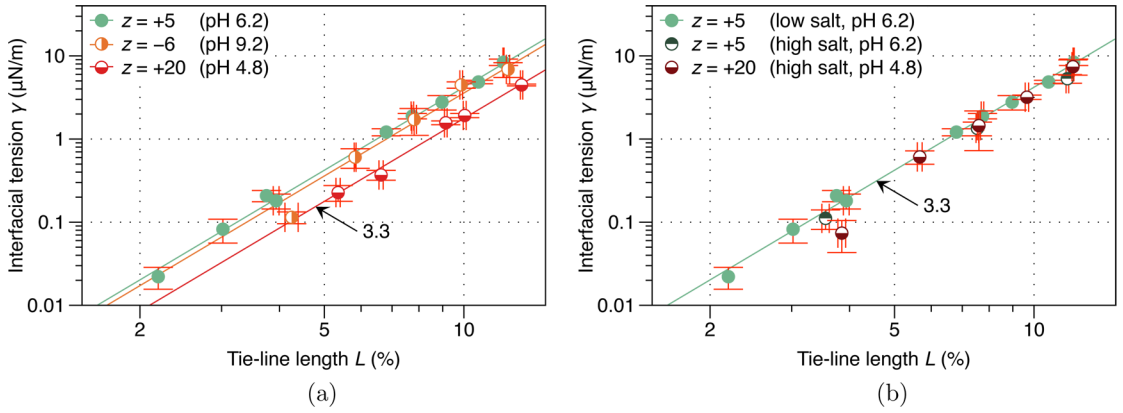

Figure 7. Measured interfacial tension γ as a function of the tie-line length L, showing the effect of (a) polyelectrolyte charge[15] (low ionic strength, 5−10 mM) and (b) the addition of 50 mM KCl. The solid lines are power-law fits with a common exponent of 3.3.

interfacial tension. More strongly increasing the magnitude of the charge to z = +20 causes a pronounced decrease in the interfacial tension by, approximately, a factor of 2. The interfacial tensions found in the presence of 50 mM KCl appear to be independent of charge and have approximately the same magnitude as for z = +5 at low ionic strength.

In order to elucidate the origin of the decrease in the interfacial tension, we used the measured Donnan potentials to calculate the change in the interfacial tension $\Delta\gamma$ as predicted by Poisson−Boltzmann theory. As the fits in Figure 6 give us the Donnan potential ψ_D as a function of the tie-line length L, inserting these fits into eq 28 gives us $\Delta\gamma$ as a function of L. By subtracting the calculated values of $\Delta\gamma$, which are always negative, from the measured interfacial tensions γ, we can assess the role of the interfacial electrical double layers in the change of the interfacial tension. In a sense, this procedure provides us with the "intrinsic" tension γ_0 of the interface, as if it were uncharged.

The resulting intrinsic interfacial tensions $\gamma_0 = \gamma - \Delta\gamma$ are shown in Figure 8. The interfacial tensions for all three values of z collapse on a single curve, which scales with a power of 3.22 ± 0.08 with the tie-line length. The exponent is found by taking the logarithm of the tension and tie-line length and performing a linear least-squares fit. We can compare these interfacial tensions with those calculated from the blob model for a mixed solution of uncharged polymers, using eq 9. The blob model shows very similar power-law scaling, with an exponent of 3.153 ± 0.005 for L in the range 2−10%. Nevertheless, the tensions predicted by the blob model are approximately a factor of 2 higher than observed in the experiments.

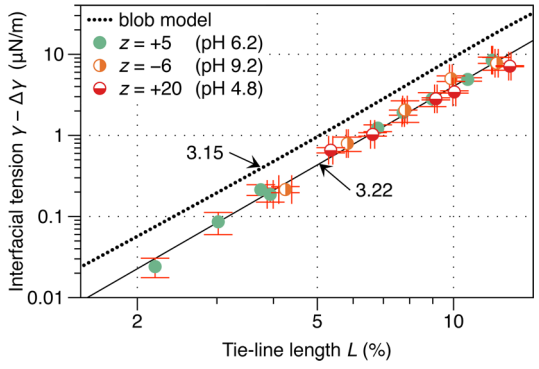

Figure 8. Measured interfacial tension γ,[15] compensated for the decrease $\Delta\gamma$ due to the interfacial electrical potential difference eq 28, as a function of the tie-line length L. The solid line is a power-law fit to all compensated experimental values, with an exponent of 3.22 ± 0.08, and the dotted line is the interfacial tension as calculated using the blob model, with an exponent of 3.153 ± 0.005.

DISCUSSION

Our detailed measurements of the Donnan potential and the interfacial tension presented in the previous section clearly show that an increase in the magnitude of the Donnan potential corresponds with a decrease in the interfacial tension at fixed tie-line length. The addition of salt suppresses the Donnan potential according to eq 31 and, as observed experimentally, also suppresses the decrease of the interfacial tension. The decrease in tension is—according to Poisson−Boltzmann theory—expected to be caused by the negative free energy of spontaneously formed electrical double layers. This free energy per unit area $\Delta\gamma$ may be calculated on the basis of measured electrical potential differences and subtracted from the measured interfacial tensions, which gives us the intrinsic interfacial tensions $\gamma - \Delta\gamma$. When plotted in this way, all points collapse onto a master curve, supporting the predicted influence of the Donnan potential on the interfacial tension.

We have evaluated the interfacial tensions in our system as a function of the tie-line length, which is a measure of the degree of phase separation. If two samples (with a different polyelectrolyte charge z, critical point, and binodal) have the same tie-line length, the difference in concentration of the two polymers between the coexisting phases is on average the same. Therefore, the fact that the intrinsic interfacial tensions as a function of the tie-line length all collapse onto a single curve indicates that the interfacial gradients remain also unchanged, despite the polymers being present at substantially different concentrations.

The interfacial tensions as calculated using the blob model are about twice as large as the measured interfacial tensions. It is to be expected that the calculated interfacial tensions are higher than those measured, since for instance monodisperse polymers are assumed in the calculations, whereas both dextran and gelatin are polydisperse. It is known that the interfacial tension of similar systems decreases with decreasing polymer molar mass, even if the same tie-line length is maintained.[35,36] As such, the presence of low-molecular weight material may reduce the interfacial tension. Additionally, in order to simplify

DOI: 10.1021/acs.macromol.5b01675
Macromolecules 2015, 48, 7335−7345

the calculations, the interfacial profile of the blob volume fraction $\eta(z)$ was optimized assuming a constant total polymer concentration throughout the interface (i.e., $\overline{u}\epsilon(z) = 0$). Only after that the profile $\overline{u}\epsilon(z)$ was optimized, assuming a fixed profile $\eta(z)$. Ideally, the two profiles would be optimized simultaneously, potentially yielding lower interfacial tensions.

A power-law scaling between the interfacial tension and tie-line length with an exponent equal to 3 may be expected from mean-field theory. When not taking into account solvent redistribution within our calculations, we find as expected an exponent 3.0451 ± 0.0014 (not shown) due to their mean-field nature. This exponent increases to 3.153 ± 0.005 when including solvent redistribution. This is similar to the exponent found experimentally (3.22 ± 0.08). Indeed, performing a *t*-test reveals that the experimental exponent is not significantly different from the calculated value.[37] The experimental exponent is, however, using the same criteria, significantly different from the value calculated without solvent redistribution. This serves as an important indication that solvent redistribution also affects the scaling of the interfacial tension experimentally.

While interfacial tensions have been reported before for similar systems,[38,39] literature data on the scaling of the interfacial tension with the tie-line length (or sometimes density difference) in comparable systems remains scarce and a range of scaling exponents has been reported. For PEG/dextran, Forciniti et al. reported numerous exponents depending on molar mass and temperature, with a mean of 3.74 ± 0.78,[35] while Bamberger et al. reported values in the range of 3.5 to 4.1[40] and Liu et al. found mean-field behavior far from the critical point.[41] Ding et al. reported a value of 2.4 for dextran/gelatin,[36] and Scholten et al. found scaling with the density difference with an exponent of 2.7 ± 0.3 for the same system.[42] Antonov et al. found an exponent of 3.1 ± 0.3 with $\Delta\rho$ for caseinate/alginate,[43] whereas Simeone et al. reported linear correlation between γ and the tie-line length or the density difference.[44] Mean-field exponents have also been reported for complex coacervates,[45,46] which are formed by oppositely charged polymers in solution. The present results show that accurate information on the scaling behavior and magnitude of the interfacial tension can be obtained by analyzing the shape of the interfacial profile.

CONCLUSION

The presence of charge on one of the polymers in coexisting solutions of polyelectrolyte and neutral polymer leads to a Donnan equilibrium and to the formation of an interfacial electrical potential difference. It is due to this Donnan potential that the interfacial tension decreases when the absolute charge of the polyelectrolyte increases, and this decrease can be understood quantitatively on the basis of Poisson−Boltzmann theory. The magnitude and scaling behavior of the interfacial tension as calculated using the blob model compare favorably with experiments. Solvent accumulation at the water/water interface has an experimentally accessible effect on the scaling behavior of the interfacial tension and can explain the experimentally observed scaling behavior.

APPENDIX

In this Appendix, we consider the general situation in which the local charge density due to presence of polyelectrolyte is *not* negligible compared to the total charge density. The total charge density is thus given by

$$\rho_e(Z) = zec^p(Z) + ec^+(Z) - ec^-(Z) \tag{A.1}$$

We shall assume that the polyelectrolyte concentration changes discontinuously from c_α^p to c_β^p at the interface ($Z = 0$). Electroneutrality dictates that there is no net charge in either bulk region, i.e.,

$$zc_\alpha^p = c_\alpha^- - c_\alpha^+ \quad \text{and} \quad zc_\beta^p = c_\beta^- - c_\beta^+ \tag{A.2}$$

For the ion density profiles, a Boltzmann distribution is assumed:

$$c^+(Z) = c_\alpha^+ \exp[-(\Psi - \Psi_\alpha)] = c_\beta^+ \exp[-(\Psi - \Psi_\beta)] \tag{A.3}$$

$$c^-(Z) = c_\alpha^- \exp[\Psi - \Psi_\alpha] = c_\beta^- \exp[\Psi - \Psi_\beta] \tag{A.4}$$

The Boltzmann assumption necessarily leads to the following two relations between the potential difference $\Psi_D = \Psi_\alpha - \Psi_\beta$ and the bulk ion densities:

$$\Psi_D = \ln(c_\beta^+/c_\alpha^+) = \ln(c_\alpha^-/c_\beta^-) \tag{A.5}$$

Using the Poisson equation, $2ec_{bulk}\, d^2\Psi/dZ^2 = -\rho_e(Z)$, the Poisson−Boltzmann equation for $\Psi(Z)$ then takes the following form:

$$\Psi''(Z) = \begin{cases} \sinh(\Psi - \Psi^\alpha) + \delta_\alpha[\cosh(\Psi - \Psi^\alpha) - 1] & (Z < 0) \\ \sinh(\Psi - \Psi^\beta) + \delta_\beta[\cosh(\Psi - \Psi^\beta) - 1] & (Z > 0) \end{cases} \tag{A.6}$$

where we have defined $\kappa_\alpha = \sqrt{8\pi\lambda_B c_\alpha}$ and $\kappa_\beta = \sqrt{8\pi\lambda_B c_\beta}$ to rescale the distance to the surface and where we have introduced:

$$c_\alpha \equiv \frac{1}{2}(c_\alpha^+ + c_\alpha^-) \quad \text{and} \quad \delta_\alpha \equiv \frac{c_\alpha^- - c_\alpha^+}{c_\alpha^+ + c_\alpha^-} = \frac{zc_\alpha^p}{c_\alpha^+ + c_\alpha^-}$$
$$c_\beta \equiv \frac{1}{2}(c_\beta^+ + c_\beta^-) \quad \text{and} \quad \delta_\beta \equiv \frac{c_\beta^- - c_\beta^+}{c_\beta^+ + c_\beta^-} = \frac{zc_\beta^p}{c_\beta^+ + c_\beta^-} \tag{A.7}$$

Note that if we neglect the polyelectrolyte charge contribution ($\delta_\alpha \approx \delta_\beta \approx 0$), the Poisson−Boltzmann equation reduces to the expression given in eq 18. The Poisson−Boltzmann equation is conveniently integrated to give

$$\frac{1}{2}(\Psi'(Z))^2 = \begin{cases} \cosh(\Psi - \Psi^\alpha) - 1 \\ \quad + \delta_\alpha[\sinh(\Psi - \Psi^\alpha) - \Psi + \Psi^\alpha] & (Z > 0) \\ \cosh(\Psi - \Psi^\beta) - 1 \\ \quad + \delta_\beta[\sinh(\Psi - \Psi^\beta) - \Psi + \Psi^\beta] & (Z < 0) \end{cases} \tag{A.8}$$

The condition of electroneutrality requires the integral over the charge density to net zero. One can show that this requirement leads to the following condition

DOI: 10.1021/acs.macromol.5b01675
Macromolecules 2015, 48, 7335−7345

$$\omega^2\left(4\sinh^2\left(\frac{\Psi^\alpha}{2}\right) - 2\delta_\alpha[\sinh(\Psi^\alpha) - \Psi^\alpha]\right) = 4\sinh^2\left(\frac{\Psi^\beta}{2}\right) - 2\delta_\beta[\sinh(\Psi^\beta) - \Psi^\beta] \tag{A.9}$$

which can be solved for Ψ^α and Ψ^β to yield:

$$\Psi^\alpha = \frac{(\omega^2 - 1)\sinh(\Psi_D) + \Psi_D[\cosh(\Psi_D) - \omega^2]}{2(\omega^2 + 1)\sinh^2(\Psi_D/2)} \tag{A.10}$$

$$\Psi^\beta = \frac{(\omega^2 - 1)\sinh(\Psi_D) + \Psi_D[1 - \omega^2\cosh(\Psi_D)]}{2(\omega^2 + 1)\sinh^2(\Psi_D/2)} \tag{A.11}$$

Furthermore, the individual ion densities in either bulk phase are given by

$$c_\alpha^+ = \frac{c_\alpha}{\sinh(\Psi_D)}\left(\frac{1}{\omega^2} - e^{-\Psi_D}\right)$$
$$c_\alpha^- = \frac{c_\alpha}{\sinh(\Psi_D)}\left(e^{\Psi_D} - \frac{1}{\omega^2}\right)$$
$$c_\beta^+ = \frac{c_\alpha}{\sinh(\Psi_D)}\left(\frac{e^{\Psi_D}}{\omega^2} - 1\right)$$
$$c_\beta^- = \frac{c_\alpha}{\sinh(\Psi_D)}\left(1 - \frac{e^{-\Psi_D}}{\omega^2}\right) \tag{A.12}$$

which leads to the following expressions for the parameters δ_α and δ_β defined in eq A.7:

$$\delta_\alpha = \frac{\cosh(\Psi_D) - 1/\omega^2}{\sinh(\Psi_D)} \quad \text{and} \quad \delta_\beta = \frac{\omega^2 - \cosh(\Psi_D)}{\sinh(\Psi_D)} \tag{A.13}$$

The electrostatic contribution to the surface tension, $\Delta\gamma$, can be calculated by integrating the surface charge over the potential as in eq 22. Alternatively, it can be determined from the general expression for the free energy in terms of the translational entropy of the ions and the electrostatic energy:

$$\Delta\gamma = \int dz \left\{\sum_i [kTc_i(z)\ln(c_i(z)) - \mu_i c_i(z)] + \frac{1}{2}\psi(z)\rho_e(z) + \Pi_{el}\right\} \tag{A.14}$$

where μ_i is the chemical potential of ion-species i and Π_{el} the osmotic pressure. The chemical potentials are determined by the requirement that the free energy is minimal in the bulk regions. This leads to

$$\frac{\mu_+}{kT} = \ln(c_\alpha^+) + 1 + \Psi_\alpha = \ln(c_\beta^+) + 1 + \Psi_\beta \tag{A.15a}$$

$$\frac{\mu_-}{kT} = \ln(c_\alpha^-) + 1 - \Psi_\alpha = \ln(c_\beta^-) + 1 - \Psi_\beta \tag{A.15b}$$

The osmotic pressures are equal in either bulk phase, $\Pi_{el} \equiv \Pi_{el}^\alpha = \Pi_{el}^\beta$, with

$$\frac{\Pi_{el}^\alpha}{kT} = c_\alpha^+ + c_\alpha^- + \Psi_\alpha[c_\alpha^+ - c_\alpha^-] \tag{A.16a}$$

$$\frac{\Pi_{el}^\beta}{kT} = c_\beta^+ + c_\beta^- + \Psi_\beta[c_\beta^+ - c_\beta^-] \tag{A.16b}$$

Using these results for μ_i and Π_{el}, the surface free energy may be written as

$$\frac{\Delta\gamma}{kT} = \kappa_\alpha^{-1}\int_{-\infty}^0 dZ\ \{c^+\ln(c^+/c_\alpha^+) + c^-\ln(c^-/c_\alpha^-) - (1 + \Psi_\alpha)[c^+ - c_\alpha^+] - (1 - \Psi_\alpha)[c^- - c_\alpha^-] + \frac{\Psi}{2}[zc_\alpha^p + c^+ - c^-]\}$$
$$+\kappa_\beta^{-1}\int_0^\infty dZ\{c^+\ln(c^+/c_\beta^+) + c^-\ln(c^-/c_\beta^-) - (1 + \Psi_\beta)[c^+ - c_\beta^+] - (1 - \Psi_\beta)[c^- - c_\beta^-] + \frac{\Psi}{2}[zc_\beta^p + c^+ - c^-]\} \tag{A.17}$$

Inserting the Boltzmann distributions and using the Poisson equation, this reduces to

$$\frac{\Delta\gamma}{kT} = \frac{c^\alpha}{\kappa_\alpha}\int_{-\infty}^0 dZ\ \{-[\Psi']^2 - 2[\cosh(\Psi - \Psi^\alpha) - 1] - 2\delta_\alpha[\sinh(\Psi - \Psi^\alpha) - \Psi + \Psi^\alpha]\}$$
$$+ \frac{c^\beta}{\kappa_\beta}\int_0^\infty dZ\ \{-[\Psi']^2 - 2[\cosh(\Psi - \Psi^\beta) - 1] - 2\delta_\beta[\sinh(\Psi - \Psi^\beta) - \Psi + \Psi^\beta]\} \tag{A.18}$$

Using the Poisson−Boltzmann equation in eq A.8, this can be written as

$$\Delta\gamma = -\frac{kT\kappa}{4\pi\lambda_B}\sqrt{\omega}\int_0^{\Psi^\alpha} d\Psi\left(4\sinh^2\left(\frac{\Psi}{2}\right) - 2\delta_\alpha[\sinh(\Psi) - \Psi]\right)^{1/2}$$
$$- \frac{kT\kappa}{4\pi\lambda_B}\frac{1}{\sqrt{\omega}}\int_{\Psi^\beta}^0 d\Psi\left(4\sinh^2\left(\frac{\Psi}{2}\right) - 2\delta_\beta[\sinh(\Psi) - \Psi]\right)^{1/2} \tag{A.19}$$

If we were to neglect the polyelectrolyte charge contribution ($\delta_\alpha \approx \delta_\beta \approx 0$), the above integrals can be evaluated and $\Delta\gamma$ reduces to the expressions in eq 23 and eq 26. Furthermore, if we assume that the Donnan potential $\Psi_D \ll 1$, we can expand in Ψ. The result is that $\omega \approx 1$ and that the terms involving δ_α and δ_β vanish to leading order so that we rederive the expression given in eq 28:

$$\Delta\gamma \simeq -\frac{kT\kappa}{16\pi\lambda_B}(\Psi_D)^2 \tag{A.20}$$

■ ASSOCIATED CONTENT

Supporting Information

The Supporting Information is available free of charge on the ACS Publications website at DOI: 10.1021/acs.macromol.5b01675.

Derivation of the profile of a liquid/liquid interface near a single vertical and list of symbols (PDF)

DOI: 10.1021/acs.macromol.5b01675
Macromolecules 2015, 48, 7335−7345

AUTHOR INFORMATION

Corresponding Authors

*(M.V.) E-mail: M.Vis@uu.nl.

*(B.H.E.) E-mail: B.H.Erne@uu.nl.

Notes

The authors declare no competing financial interest.

ACKNOWLEDGMENTS

This work was supported by The Netherlands Organisation for Scientific Research (NWO).

REFERENCES

(1) Flory, P. J. *Principles of Polymer Chemistry*; Cornell University Press: Ithaca, NY, 1953.

(2) Beijerinck, M. W. *Zentralbl. Bakteriol., Parasitenkd. Infektionskrankh.* **1896**, *22*, 697−699.

(3) Albertsson, P.-Å. *Nature* **1958**, *182*, 709−711.

(4) Bungenberg de Jong, H. G.; Kruyt, H. R. *Proc. K. Ned. Akad. Wet.* **1929**, *32*, 849−856.

(5) Broseta, D.; Leibler, L.; Kaddour, L. O.; Strazielle, C. *J. Chem. Phys.* **1987**, *87*, 7248.

(6) Donnan, F. G. *Z. Elektrochem. Angew. Phys. Chem.* **1911**, *17*, 572−581.

(7) Donnan, F. G. *Chem. Rev.* **1924**, *1*, 73−90.

(8) Bergfeldt, K.; Piculell, L. *J. Phys. Chem.* **1996**, *100*, 5935−5940.

(9) Vis, M.; Peters, V. F. D.; Tromp, R. H.; Erné, B. H. *Langmuir* **2014**, *30*, 5755−5762.

(10) Borue, V. Y.; Erukhimovich, I. Y. *Macromolecules* **1988**, *21*, 3240−3249.

(11) Joanny, J. F.; Leibler, L. *J. Phys. France* **1990**, *51*, 545−557.

(12) Nyrkova, I. A.; Khokhlov, A. R.; Doi, M. *Macromolecules* **1994**, *27*, 4220−4230.

(13) de Hoog, E. H. A.; Tromp, R. H. *Colloids Surf. A* **2003**, *213*, 221−234.

(14) Tolstoguzov, V. *Food Hydrocolloids* **2003**, *17*, 1−23.

(15) Vis, M.; Peters, V. F. D.; Blokhuis, E. M.; Lekkerkerker, H. N. W.; Erné, B. H.; Tromp, R. H. *Phys. Rev. Lett.* **2015**, *115*, 078303.

(16) Broseta, D.; Leibler, L.; Joanny, J. F. *Macromolecules* **1987**, *20*, 1935−1943.

(17) Broseta, D.; Leibler, L.; Lapp, A.; Strazielle, C. *Europhys. Lett.* **1986**, *2*, 733.

(18) Tromp, R. H.; Blokhuis, E. M. *Macromolecules* **2013**, *46*, 3639−3647.

(19) Tromp, R. H.; Vis, M.; Erné, B. H.; Blokhuis, E. M. *J. Phys.: Condens. Matter* **2014**, *26*, 464101.

(20) Granath, K. A. *J. Colloid Sci.* **1958**, *13*, 308−328.

(21) Lide, D. R., Ed. *CRC Handbook of Chemistry and Physics*, 90th ed.; CRC Press: Boca Raton, FL, 2009.

(22) Widom, B.; Rowlinson, J. S. *Molecular Theory of Capillarity*; Oxford University Press: Oxford, U.K., 1984.

(23) Verwey, E. J. W.; Overbeek, J. T. G. *Theory of the stability of lyophobic colloids*; Dover Publications: New York, 1999.

(24) Frenkel, J. *Kinetic Theory of Liquids*; Dover Publications: New York, 1955.

(25) Ruckenstein, E.; Krishnan, R. *J. Colloid Interface Sci.* **1980**, *76*, 201−211.

(26) Ohshima, H.; Ohki, S. *J. Colloid Interface Sci.* **1985**, *103*, 85−94.

(27) Volkov, A. G.; Deamer, D. W.; Tanelian, D. L.; Markin, V. S. *Prog. Surf. Sci.* **1996**, *53*, 1−134.

(28) Vis, M.; Peters, V. F. D.; Erné, B. H.; Tromp, R. H. *Macromolecules* **2015**, *48*, 2819−2828.

(29) Aarts, D. G. A. L.; van der Wiel, J.; Lekkerkerker, H. N. W. *J. Phys.: Condens. Matter* **2003**, *15*, S245−S250.

(30) Scholten, E.; Sagis, L. M. C.; van der Linden, E. *Biomacromolecules* **2006**, *7*, 2224−2229.

(31) Antonov, Y. A.; Van Puyvelde, P.; Moldenaers, P.; Leuven, K. U. *Biomacromolecules* **2004**, *5*, 276−283.

(32) Batchelor, G. K. *An Introduction to Fluid Dynamics*; Cambridge University Press: Cambridge, U.K., 2002.

(33) Overbeek, J. T. G. *J. Colloid Sci.* **1953**, *8*, 593−605.

(34) Overbeek, J. T. G. *Prog. Biophys. Biophys. Chem.* **1956**, *6*, 58−84.

(35) Forciniti, D.; Hall, C. K.; Kula, M. R. *J. Biotechnol.* **1990**, *16*, 279−296.

(36) Ding, P.; Wolf, B.; Frith, W. J.; Clark, A. H.; Norton, I. T.; Pacek, A. W. *J. Colloid Interface Sci.* **2002**, *253*, 367−376.

(37) The *t*-test was performed using the 19 measurements resulting in 17 degrees of freedom, confidence level 95%, neglecting the standard deviation in the exponent from theory.

(38) Langhammer, V. G.; Nestler, L. *Makromol. Chem.* **1965**, *88*, 179−187.

(39) Ryden, J.; Albertsson, P.-Å. *J. Colloid Interface Sci.* **1971**, *37*, 219−222.

(40) Bamberger, S.; Seaman, G. V.; Sharp, K. A.; Brooks, D. E. *J. Colloid Interface Sci.* **1984**, *99*, 194−200.

(41) Liu, Y.; Lipowsky, R.; Dimova, R. *Langmuir* **2012**, *28*, 3831−3839.

(42) Scholten, E.; Tuinier, R.; Tromp, R. H.; Lekkerkerker, H. N. W. *Langmuir* **2002**, *18*, 2234−2238.

(43) Antonov, Y. A.; Van Puyvelde, P.; Moldenaers, P. *Int. J. Biol. Macromol.* **2004**, *34*, 29−35.

(44) Simeone, M.; Alfani, A.; Guido, S. *Food Hydrocolloids* **2004**, *18*, 463−470.

(45) Spruijt, E.; Sprakel, J.; Cohen Stuart, M.; van der Gucht, J. *Soft Matter* **2010**, *6*, 172−178.

(46) Qin, J.; Priftis, D.; Farina, R.; Perry, S. L.; Leon, L.; Whitmer, J.; Hoffmann, K.; Tirrell, M.; de Pablo, J. J. *ACS Macro Lett.* **2014**, *3*, 565−568.

DOI: 10.1021/acs.macromol.5b01675
Macromolecules 2015, 48, 7335−7345